Production of annular flat-topped vortex beams

Jiannong Chen (陈建农)*, Yongjiang Yu (于永江), and Feifei Wang (王菲菲)

School of Physics, Ludong University, Yantai 264025, China

**Corresponding author: jnchen1963@yahoo.com.cn*

Received October 12, 2010; accepted November 17, 2010; posted online January 1, 2011

A model of an annular flat-topped vortex beam based on multi-Gaussian superimposition is proposed. We experimentally produce this beam with a computer-generated hologram (CGH) displayed on a spatial light modulator (SLM). The power of the beam is concentrated on a single-ring structure and has an extremely strong radial intensity gradient. This beam facilitates various applications ranging from Sisyphus atom cooling to micro-particle trapping.

OCIS codes: 090.1760, 140.3300, 140.3320.

doi: 10.3788/COL201109.011402.

In optical trapping, the dark hollow beam is a powerful tool because it possesses many unique features, such as zero center intensity, orbital angular momentum, strong intensity gradient force, and propagation invariance. The most attractive and practical applications of dark hollow beams include atom manipulations, such as atom transport, atom guiding, evaporative cooling, and dipole trapping[1−8]. These atom manipulations and applications require the optical gradient force to restrict the transverse motion of the atoms. For the gradient force, the frequency detuning of the laser light can either attract or repel the atoms from regions of high light intensity. In red-detuned guiding, the atoms are attracted to the maximum intensity of the light beam. However, this form of guiding has drawbacks mainly in the form of heating resulting from spontaneous emission as the atoms spend an extensive period of time in regions of high light intensity. This heating invariably leads to the loss of coherence and an increase in average temperature of the atomic ensemble. Blue-detuned guiding, in which the light frequency is tuned above resonance, is advantageous in this respect because the atoms are restricted to regions of intensity minima. Thus, perturbations induced by the light field are minimized. Dark hollow beams also show promise for the long-distance transport of large numbers of ultra-cold atoms, making them strong competitors against hollow fiber atom guides, because a dark hollow beam may guide cold atoms along hollow fibers. Guiding along hollow fibers has been reported in both the red- and blue-detuned regimes[9−11]. Dark hollow beams, however, have some significant advantages over the use of hollow fibers, such as the ease with which they are loaded, physical wall elimination, and the variation of core size.

Well-known dark hollow beams include the Laguerre-Gaussian (LG) and Bessel beams. These beams have been intensively studied, both theoretically and experimentally[12−15]. More importantly, higher order forms of these beams retain their on-axis intensity minimum and are very well suited for atom guiding and atom optics. In addition, high-order Bessel light beams are better candidates for atom guiding over extended distances due to their non-diffractive nature and very narrow dark central regions. LG beams with higher azimuthal index l concentrate their power in a narrower ring, resulting in steeper and larger potential barriers; such beams with higher radial index p present more radial intensity nodes, resulting in widening multi-ringed power distribution. However, LG beams are inferior to high-order Bessel beams in terms of propagation invariance, narrow dark central region, and potential barrier. Arlt *et al.* reported a method for directly transforming a LG beam into a higher order Bessel beam using an axicon; in that work, the hole drilled into the axicon allows a cold atomic beam to be directly channeled into the Bessel beam guide[6].

In the case of the Gaussian beam, the forces exerted on the micro-particles are scattering and gradient forces. The scattering force usually weakens the effect of the

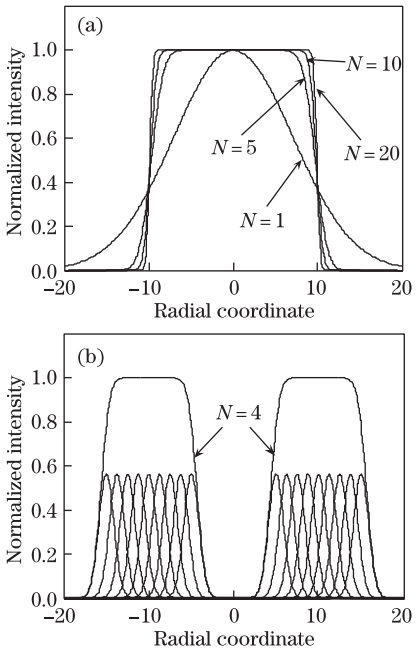

Fig. 1. One-dimensional radial intensity distribution simulation of the mathematical model for the multi-Gaussian beam. (a) Demonstration of the effect of large number N; when N becomes large, the superimposed multi-Gaussian beam tends to become a flat-topped beam with the center located at the origin of the radial coordinate. (b) Radial normalized intensity distributions for annular flat-topped vortex beams and their individual Gaussian component beams.

gradient trapping force. Dark hollow beams have no axial scattering force, which is instrumental in enhancing the trapping effect. The crucial factor for successful applications of dark hollow beams is the strong intensity gradient of inner boundaries. However, the maximum gradient force in the LG, Bessel-Gaussian, and doughnut-like beams is limited when the total laser power is set, because these beams have fixed transverse intensity profiles. Alternate beams with extremely strong intensity gradients are eagerly sought by physicists[16−18]. Monte-Carlo simulations and experimental research show that the intensity gradient is usually small and inefficient for Sisyphus atom cooling, either in standing or evanescent wave[19,20].

In this letter, we demonstrate a method of producing an annular flat-topped vortex beam, which has a stronger intensity gradient than any current beam profile. The method involves a computer-generated hologram (CGH) displayed on a nematic liquid crystal spatial light modulator (SLM). The hologram is formed by interference between the inclined incident plane reference beam and the annular flat-topped vortex object beam. This robust beam possesses the strongest intensity gradient and all power concentrated on single-ring can be used to cool, guide, and rotate atoms.

The mathematical model for the object beam we adopt is multi-Gaussian written as:

$$E(r,\phi) = E_0 \frac{\sum_{n=-N}^{N} \exp\left[-\left(\frac{r-r_0-nw_0}{w_0}\right)^2\right]}{\sum_{n=-N}^{N} \exp(-n^2)} \cdot \exp(\mathrm{i}m\phi), \quad (1)$$

where E_0 is a constant; r and ϕ are polar coordinates; r_0 is a radial location biased value controlling the size of the central dark area; m is the topological charge of vortex beam; N is referred to as the order of the multi-Gaussian beam, when $N = 0$, the multi-Gaussian beam reduces to the fundamental Gaussian beam; w_0 is the width of the individual Gaussian beam. The width of the entire multi-Gaussian beam W is related to w_0 by

$$w_0 = \frac{W}{N + \left\{1 - \ln\left[\sum_{n=-N}^{N} \exp(-n^2)\right]\right\}^{1/2}}. \quad (2)$$

The multi-Gaussian beam model expressed in Eq. (1) may be taken as the superimposition of $2N+1$ individual Gaussian vortex beams, each of which is radially centered on $r_0 + nw_0$. The one-dimensional (1D) radial intensity profiles with different N and the individual Gaussian component are illustrated in Figs. 1(a) and (b) along with their superimposed annular flat-topped beams. According to Eq. (2), if we design a multi-Gaussian beam with $W = 10$ and N takes 10 or 20, then w_0 should take either 0.4842 or 0.9382. With an increased order of the multi-Gaussian beam, the intensity gradients of the superimposed multi-Gaussian beam or annular flat-topped vortex beam at the boundaries become large, which is a requirement in neutral atom Sisyphus cooling. When N approaches infinity, the annular flat-topped vortex beam becomes an ideal flat-topped beam. Figures 2(a) and (b) show the calculated intensity and phase distribution of annular flat-topped vortex beams. The main parameters are $N = 8$ and $m = 5$, which verify the feasibility of the mathematical model for the annular flat-topped vortex beam.

To experimentally produce the annular flat-topped vortex beam, we used a digital holography scheme. An inclined incident plane wave was taken as the reference beam described by $E(x) = E_0 \exp(\mathrm{i}2\pi\alpha/\lambda)$, where α is the directional cosine, and λ is the laser wavelength. The object beam was the annular flat-topped vortex beam we want to produce. Figure 2(c) shows one example of the interfergram. There are complex fork gratings and thick fringes, and there are numerous fine fringe structures on each of the thick fringes resulting from the specific structure of object wave. Figure 2(d) is the computer-reconstructed intensity profile of the annular flat-topped vortex beam, which has been directly obtained by applying discrete fast Fourier transform to the interfergram. In the experiment, the emitting source was the He-Ne laser with a wavelength of 632.8 nm; it was pinhole-filtered, collimated, and directed onto the nematic liquid crystal SLM, as shown in Fig. 3(a). The total pixel number was 1024×768, and the pixel size was 14×14 (μm). Two linear polarizers were placed in front of and behind the SLM, respectively. The calculated hologram from the computer was displayed on SLM through a cable connection. To optimize the visibility of the interfergram and use the gray level available on the SLM, we carefully selected an amplification coefficient to alter the gray level of the whole hologram. Changing the relative azimuthal angle through rotating two polarizers, the diffraction efficiency is improved. If the diffracting images of different orders were not spatially separated, the direction cosine had to be slightly adjusted. To realize far-field Fraunhofer diffraction observation, a lens was inserted somewhere behind the SLM, and the charge-coupled device (CCD) was focused on the focal plane of the lens. However, we observed that the annular beam quality

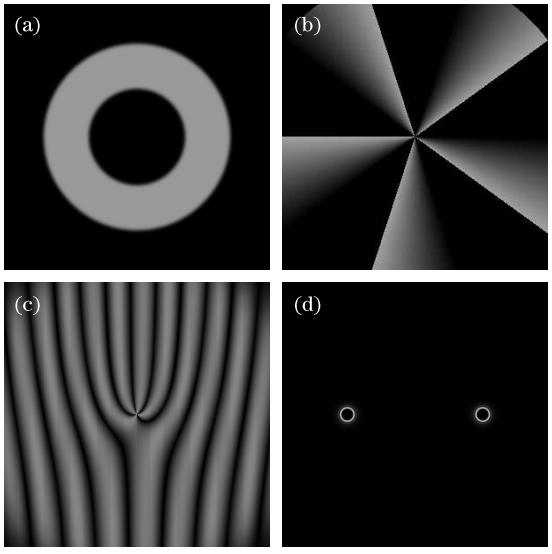

Fig. 2. Calculated (a) intensity distribution and (b) phase distribution of annular flat-topped vortex beams. (c) CGH and (d) its reconstructed image.

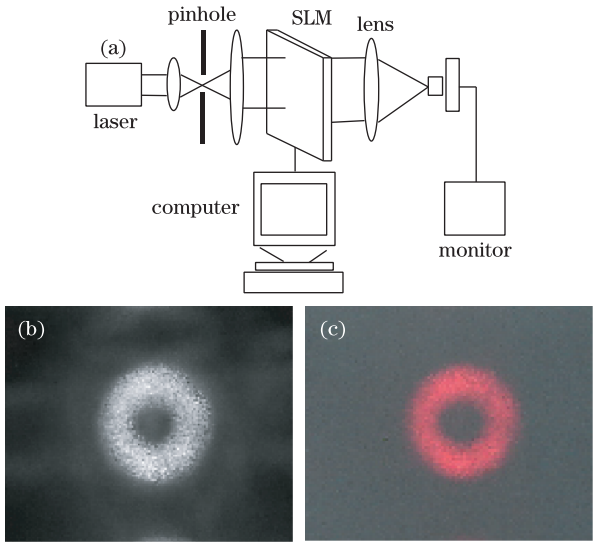

Fig. 3. (a) Experimental setup for producing the annular flat-topped vortex beams; (b) reconstructed annular flat-topped vortex beams taken in black-white camera mode; (c) reconstructed annular flat-topped vortex beams taken in color camera mode.

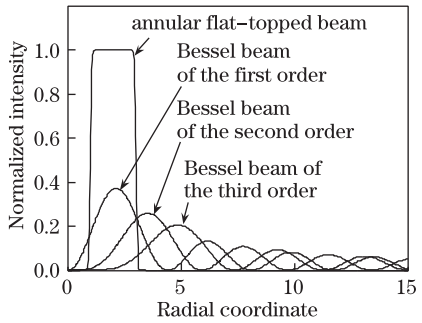

Fig. 4. Radial intensity distributions of the annular flat-topped beam and the high-order Bessel beam.

was damaged. To minimize the influence of the imaging system and the lens on the reconstructed annular flat-topped vortex beam, we removed the lens and illuminated the SLM with a slightly converging collimated beam. Afterwards, we observed the reconstructed annular flat-topped vortex beam 2 m away from the SLM. Figures 3(b) and (c) show the pictures taken from this plane. As can be seen, it is a single-ring beam with a good flat top intensity; in addition, the inner boundary has a clear and sharp edge, which is useful in firmly trapping the atoms and making it difficult for them to escape. The resulting image is much clearer than the one displayed on the monitor. As designed, the light intensity in the nearby axis was nearly zero, which exerted no radiation pressure on the trapped atoms. In other words, the light intensity in the nearby axis did not perturb the cooled atoms; the intensity variations around the flat-topped ring and the annular width deformation (Figs. 3(b) and (c)) were caused by the misalignment of the whole optical system. These intensity variations around the ring resulted in the azimuthal component of the gradient force. The misalignment also led to the breakdown of the vortex and the loss of circularly symmetrical intensity profile. To ensure a perfect annular flat-topped vortex beam, careful alignment and adjustment are critically needed.

In the process of creating a CGH, the central dark areas can be controlled by adjusting the annulus radius. In this work, the central dark area was reduced by employing a telescope in the reconstructed beam. Thus, the reconstructed dark hollow beam had a dark center, which was as small as we wanted. The reduced dark center area implies that more energy is concentrated on the flat-topped ring. A dark center, which is as small as the magnitude of wavelength, exhibits some significant features. The width of the annulus is controllable by altering the number of individual Gaussian beam; in the case of a wide annulus, it renders lasting dragging force to the trapped particles or cooled atoms to prevent them from escaping from the trap or light conduit when the light beam moves transversely. However, when the beam is blue-detuned, the atoms are attracted to the dark center area, and in this case, a wide annulus is not preferred.

To understand the superiority of a single-ring structure of an annular flat-topped beam compared with a high-order Bessel beam in terms of energy efficiency, we illustrated the radial intensity distribution of both beams with approximately equal total energy (Fig. 4). As each ring of a high-order Bessel beam contains equal portion of total laser energy[21], the innermost ring playing a dominant role in trapping, guiding, cooling, and rotating atoms has the highest energy density due to the short ring radius. However, the innermost ring of the high-order Bessel beam only accounts for a very small fraction of the total energy, compared with the single-ring flat-topped beam with the same total energy.

This annular flat-topped beam is a vortex beam containing spiral phase term $\exp(\mathrm{i}m\phi)$, which makes the center point a phase singularity. Electromagnetic radiation with spiral phase distribution and linear polarization possesses orbital angular momentum and spin angular momentum. Each photon in the beam contains $m\hbar$ of the orbital angular momentum. Orbital angular momentum and spin angular momentum can be transferred to microparticles and cold atoms[22−24]; therefore, the annular flat-topped vortex beam will truly be an optical spanner capable of rotating the trapped atoms.

In conclusion, we have proposed a mathematical model for annular flat-topped vortex beams, which is a superimposition of multi-Gaussian beams. With enough number of individual Gaussian beams and a small waist width, the annular flat-topped vortex beams will have an intensity gradient, which will be as strong as desired. Experimentally, we have produced the annular flat-topped vortex beams using a CGH displayed on a nematic liquid crystal SLM. The produced annular flat-topped vortex beams agree well with the theoretical expectation. Due to its single-ring intensity profile, the energy efficiency is much higher than those of the well-known LG beam and Bessel beam in application and in production. The annular flat-topped vortex beams with a strong intensity gradient are suitable for firmly trapping, cooling, and guiding particles, especially atoms. Furthermore, the photons in the beams carry orbital angular momentum, making the annular flat-topped vortex beams capable of rotating particles.

This work was supported by the National Natural Science Foundation of China (No. 11074105), the Natural Science Foundation of Shandong Province (No. Z2008A02), and the Ludong University Natural Science Doctorate Program (No. LY20082802).

References

1. S. Chu, J. E. Bjorkholm, A. Ashkin, and A. Cable, Phys. Rev. Lett. **57,** 314 (1986).
2. E. L. Raab, M. Prentiss, A. Cable, S. Chu, and D. E. Pritchard, Phys. Rev. Lett. **59,** 2631 (1987).
3. Y. Song, D. Milam, and W. T. Hill III, Opt. Lett. **24,** 1805 (1999).
4. T. L. Gustavson, A. P. Chikkatur, A. E. Leanhardt, A. Görlitz, S. Gupta, D. E. Pritchard, and W. Ketterle, Phys. Rev. Lett. **88,** 020401 (2002).
5. S. Kuppens, M. Rauner, M. Schiffer, K. Sengstock, W. Ertmer, F. E. van Dorsselaer, and G. Nienhuis, Phys. Rev. A **58,** 3068 (1998).
6. J. Arlt, T. Hitomi, and K. Dholakia, Appl. Phys. B **71,** 549 (2000).
7. G. Wang, W. Ji, J. Ma, L. Wang, L. Xiao, and S. Jia, Chinese J. Lasers (in Chinese) **35,** 221 (2008).
8. L. Chen and J. Yin, Acta Opt. Sin. (in Chinese) **30,** 1217 (2010).
9. M. J. Renn, D. Montgomery, O. Vdovin, D. Z. Anderson, C. E. Wieman, and E. A. Cornell, Phys. Rev. Lett. **75,** 3253 (1995).
10. M. J. Renn, E. A. Donley, E. A. Cornell, C. E. Wieman, and D. Z. Anderson, Phys. Rev. A **53,** R648 (1996).
11. H. Ito, T. Nakata, K. Sakaki, M. Ohtsu, K. I. Lee, and W. Jhe, Phys. Rev. Lett. **76,** 4500 (1996).
12. M. A. Clifford, J. Arlt, J. Courtial, and K Dholakia, Opt. Commun. **156,** 300 (1998).
13. A. Vasara, J. Turunen, and A. T. Friberg, J. Opt. Soc. Am. A **6**, 1748 (1989).
14. L. Allen, M. W. Beijersbergen, R. J. C. Spreeuw, and J. P. Woerdman, Phys. Rev. A **45,** 8185 (1992).
15. C. Paterson and R. Smith, Opt. Commun. **124,** 121 (1996).
16. D. J. Wineland, J. Dalibard, and C. Cohen-Tannoudji, J. Opt. Soc. Am. B **9,** 32 (1992).
17. H. Nha and W. Jhe, Phys. Rev. A **56,** 729 (1997).
18. M. Grajcar, S. H. W. van der Ploeg, A. Izmalkov, E. Il'ichev, H.-G. Meyer, A. Fedorov, A. Shnirman, and G. Schön, Nature Phys. **4,** 612 (2008).
19. Yu. B. Ovchinnikov, L. Manek, A. I. Sidorov, G. Wasik, and R. Grimm, Europhys. Lett. **43,** 510 (1998).
20. J. Yin, W. Gao, Y. Wang, and Y. Wang, Phys. Lett. A **288,** 9 (2001).
21. K. Volke-Sepulveda, V. Garcés-Chávez, S. Chávez-Cerda, J. Arlt, and K. Dholakia, J. Opt. B: Quantum Semiclass. Opt. **4,** S82 (2002).
22. J. W. R. Tabosa and D. V. Petrov, Phys. Rev. Lett. **83,** 4967 (1999).
23. M. E. J. Friese, J. Enger, H. Rubinsztein-Dunlop, and N. R. Heckenberg, Phys. Rev. A **54,** R1593 (1996).
24. Q. Gao, Y. Zhu, J. Shi, Y. Li, M. Wang, and Y. Wei, Chinese J. Lasers (in Chinese) **35,** 1505 (2008).